catalysts

MDPI

Article

# Intrinsic Activity of $MnO_x$-$CeO_2$ Catalysts in Ethanol Oxidation

**Dimitrios Delimaris and Theophilos Ioannides ***

Foundation for Research & Technology-Hellas, Institute of Chemical Engineering Sciences (FORTH/ICE-HT), Stadiou str., Platani, 26504 Patras, Greece; jimdelmar@gmail.com

* Correspondence: theo@iceht.forth.gr; Tel.: +30-2610-965-264

Received: 4 October 2017; Accepted: 8 November 2017; Published: 10 November 2017

**Abstract:** $MnO_x$-$CeO_2$ mixed oxides are considered efficient oxidation catalysts superior to the corresponding single oxides. Although these oxides have been the subject of numerous studies, their fundamental performance indicators, such as turnover frequency (TOF) or specific activity, are scarcely reported. The purpose of the present work is to investigate the effect of catalyst composition on the concentration of active sites and intrinsic activity in ethanol oxidation by the employment of temperature-programmed desorption and oxidation of isotopically-labelled ethanol, $^{12}CH_3{}^{13}CH_2OH$. The transformation pathways of preadsorbed ethanol in the absence of gaseous oxygen refer to dehydrogenation to acetaldehyde followed by its dissociation combined with oxidation by lattice oxygen. In the presence of gaseous oxygen, lattice oxygen is rapidly restored and the main products are acetaldehyde, $CO_2$, and water. $CO_2$ forms less easily on mixed oxides than on pure $MnO_x$. The TOF of ethanol oxidation has been calculated assuming that the amount of adsorbed ethanol and $CO_2$ produced during temperature-programmed oxidation (TPO) is a reliable indicator of the concentration of the active sites.

**Keywords:** ethanol; ceria; manganese; oxidation; temperature-programmed desorption; TOF

## 1. Introduction

Volatile organic compounds (VOCs) include all organic compounds that exist in the gaseous state in air. Ethanol is one of the dominating VOCs in some segments of the printing industry and in exhaust gases from ethanol-fuelled vehicles. The most commonly employed methods for ethanol (total) oxidation are thermal and catalytic incineration [1]. Noble metals [2–4] and oxides of the transition metals [5–7] have been mostly investigated for the complete oxidation of ethanol.

The possibility of forming partial oxidation products that are more harmful than the original organic compound is very high during the oxidation process of compounds like ethanol. Side reactions are mainly dehydrogenation to acetaldehyde and dehydration to ethylene or diethyl ether [4,8]. In some cases, due to secondary reactions of these primary products, the formation of molecules with more than two carbon atoms, such as ethyl acetate, crotonaldehyde, and acetone has been reported [9,10].

The interaction of ethanol with ceria-based catalysts including ceria-supported metals (Pd, Pt, Rh, and Co) has been studied with dynamic techniques, such as temperature-programmed desorption (TPD), by several investigators [10–13]. It has been generally observed that a part of ethanol reversibly adsorbs and desorbs at low temperatures, while the remaining part undergoes surface transformation to other surface species. Acetaldehyde is a major desorption product over $CeO_2$ and $Rh/CeO_2$, while it is produced in small amounts over $Pt/CeO_2$ and $Pd/CeO_2$. CO and $CO_2$ are other major desorption products and the formation of methane, benzene, and acetone has also been reported. In the case of $Co/CeO_2$, the main products during TPD were $CH_3CHO$, $C_2H_4$, and $CH_4$ [13].

A common approach to enhance the catalytic function of ceria in oxidation reactions is the addition of a dopant cation towards a mixed metal oxide. If the dopant is $Mn^{n+}$, whose corresponding

oxides ($Mn_3O_4$, $Mn_2O_3$, $MnO_2$) are among the most active in VOC oxidation, the resulting $Mn_xCe_{1-x}O_\delta$ materials, either cerium-rich or manganese-rich, are interesting candidate catalysts. Several investigators have reported on the performance of $MnO_x$-$CeO_2$ catalysts in VOC oxidation. The morphological impact of manganese–cerium oxides on ethanol oxidation has been examined by Li et al. [14]. They showed that different crystallographic faces possess different oxidation activities. The oxidation of ethanol over $Mn_{0.6}Ce_{0.4}O_2$ prepared by coprecipitation leads to acetaldehyde and $CO_2$ as oxidation products and complete conversion to $CO_2$ is achieved at temperatures around 200 °C [15]. The oxidation of benzene over Ce–Mn oxides synthesized by flame spray pyrolysis has been examined by Liu et al. [16]. The 12.5%-Ce–Mn oxide was the most active sample. The oxidation of toluene over nanorod-shaped Mn-Ce mixed oxides prepared by hydrothermal treatment was studied by Liao et al. [17]. The highest activity was observed for the samples with a high manganese content. Mn-Ce mixed oxides prepared by an oxalate precursor were examined in the oxidation of benzene, toluene, and ethyl acetate by Tang et al. [18,19]. Mn-Ce mixed oxides prepared by coprecipitation were studied in the oxidation of n-hexane by Picasso et al. [20]. The $Ce_{0.67}Mn_{0.33}O_2$ with a 24 h aging time showed the highest performance. Mn-Ce mixed oxides synthesized via a modified reverse nanoemulsion method were investigated in the oxidation of methanol [21]. The highest activity was shown by the monophasic $Mn_{0.25}Ce_{0.75}O_2$ catalyst. Mn-Ce mixed oxides have also been examined in diesel soot oxidation [22]. The most active sample was the one containing 20 at.% Mn. Single and mixed Mn-Ce oxides supported in ceramic monoliths were applied in the oxidation of toluene, ethanol, and methyl ethyl ketone [23]. The Mn-rich mixed oxide exhibited the best performance. Pintos et al. have performed density functional theory (DFT+U) calculations to gain insight into the behavior of a 12.5% Mn-doped $CeO_2$ solid solution in oxidation reactions [24]. We have reported on the performance of a series of $MnO_x$-$CeO_2$ catalysts, prepared by the urea combustion method, in ethanol oxidation [8]. An interesting finding of that study was that mixed oxide catalysts present smaller specific activity than the single oxide counterparts ($MnO_x$, $CeO_2$), but the larger surface area of mixed oxide catalysts counterbalances their smaller specific activity allowing complete conversion of the examined VOCs at lower temperatures compared to the single oxides. Using standard definitions, as found, e.g., in [25], the reaction rate, R, over a catalyst can be expressed as the product of turnover frequency, TOF, concentration of active sites on the catalyst surface, $C_{sites}$, and the specific surface area of the catalyst, SSA, as follows:

$$R\ (mol\ s^{-1}\ g^{-1}) = TOF\ (s^{-1})\ C_{sites}(mol\ m^{-2})\ SSA\ (m^2\ g^{-1}) \quad (1)$$

The observed decrease in specific activity could be due to smaller TOF or $C_{sites}$ values or both in the mixed oxides. In order to gain more information on the nature of surface processes and transformation steps of adsorbed ethanol, which are considered relevant to the kinetics of ethanol oxidation over $MnO_x$-$CeO_2$ catalysts, a study of temperature-programmed desorption (TPD) and oxidation (TPO) of isotope-labelled ethanol was carried out, the results of which are the subject of the present work.

## 2. Results

Catalyst characterization results have been reported elsewhere [8]. In brief, it was found that a major fraction of Mn ions get incorporated in the ceria lattice with a homogeneous distribution of Mn ions in the bulk and the surface for Mn/(Mn + Ce) ratios up to 0.25. At Mn/(Mn + Ce) ratios higher than 0.25, the segregation of a separate $Mn_3O_4$ phase took place. The specific surface areas of mixed oxide samples were up to one order of magnitude higher than the ones of pure $CeO_2$ or $MnO_x$.

### *2.1. TPD of Ethanol*

Temperature programmed desorption profiles of ethanol over pure $CeO_2$ and pure $MnO_x$ are presented in Figure 1. Molecular ethanol ($^{12}CH_3{}^{13}CH_2OH$) was desorbed in the form of two or three overlapping peaks at temperatures below 200 °C. Desorption of ethanol from $CeO_2$ or M/$CeO_2$

catalysts in the form of one or more overlapping peaks below 200 °C has also been observed by other investigators [11,12,26]. At the same temperature region (below 200 °C), acetaldehyde desorption was observed. The production of acetaldehyde is accompanied by water production indicative of the participation of oxygen from the catalyst surface according to the overall reaction:

$$[C_2H_5OH] + [O] \rightarrow CH_3CHO + H_2O \quad (2)$$

Decomposition and oxidation reactions of the adsorbed ethanol take place at temperatures above 230 °C leading to the production of $CO_2$, CO, $^{13}CO_2$, $^{13}CO$, $H_2$, and $H_2O$ in the case of $CeO_2$. CO and $^{13}CO$ appear in the form of three peaks at 300, 430, and 630 °C. The low-temperature CO peak is accompanied by $H_2$ desorption. The relative intensity of the three peaks is different for $^{12}CO$ and $^{13}CO$ with most $^{13}CO$ located in the low-temperate peak compared to $^{12}CO$. This is understandable taking into account that $^{13}CO$ originates from the labelled $\alpha$-carbon of ethanol. The presence of $^{12}CO$ indicates the oxidation of β-carbon of the original adsorbed ethanol molecule. Noting that above 230 °C no intact ethanol molecule is expected to remain on the ceria surface, the observed family of peaks at 300 °C ($^{12}CO$, $H_2$, $^{13}CO$) can be attributed to oxidative decomposition of adsorbed acetaldehyde-like species:

$$[^{12}CH_3{}^{13}CHO] + [O] \rightarrow {}^{12}CO + {}^{13}CO + H_2 + H_2O \quad (3)$$

It should be noted that no $CH_4$ ($m/z$ = 15) was detected to desorb during TPD. The presence of CO at higher temperatures indicates that the lattice oxygen of ceria is not readily available to fully oxidize all carbon species originating from ethanol. $^{12}CO_2$ and $^{13}CO_2$ have similar profiles in the form of two peaks at 350–400 °C and 600–700 °C. Overall, the complexity of the TPD profiles over $CeO_2$ indicates the presence of a multitude of adsorption states and intermediate species. The fact, though, that the profiles of $^{12}C$ and $^{13}C$-containing molecules are similar implies that these adsorbed species contain (at least) one C-C bond whose breaking is rate determining.

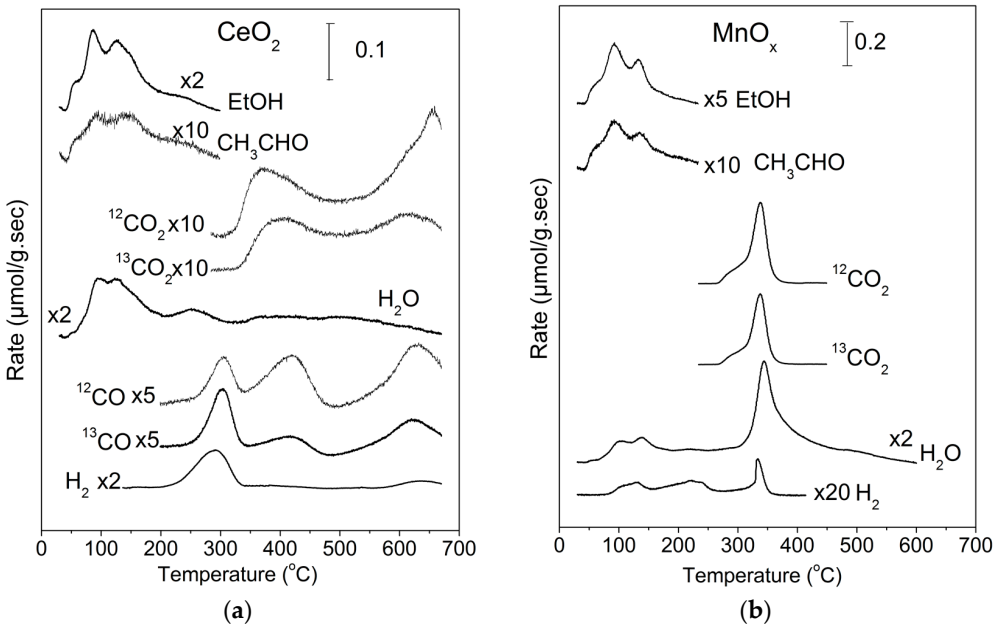


**Figure 1.** (**a**) TPD profiles following $^{12}CH_3{}^{13}CH_2OH$ adsorption on pure $CeO_2$, (**b**) TPD profiles following $^{12}CH_3{}^{13}CH_2OH$ adsorption on pure $MnO_x$.

The corresponding TPD profile following $^{12}CH_3{}^{13}CH_2OH$ adsorption on pure $MnO_x$ is presented in Figure 2b. Molecular desorption of ethanol is observed in the form of three overlapping peaks at temperatures below 200 °C accompanied by similar in shape acetaldehyde peaks. In contrast to

what was found in the case of $CeO_2$, no CO (either $^{12}CO$ or $^{13}CO$) was detected to desorb during TPD. This is an indication of a higher oxidation capability of $MnO_x$ compared to $CeO_2$. The profile is also simpler with a single peak of $CO_2$ with a small hump at the low-temperature side. The $CO_2$ peak, which is accompanied by a $H_2O$ peak, is at ~340 °C compared to the double peaks at 350–400 °C and 600–700 °C in the case of $CeO_2$.

TPD profiles from $Mn_{0.25}Ce_{0.75}$ and $Mn_{0.75}Ce_{0.25}$ catalysts following $^{12}CH_3{}^{13}CH_2OH$ adsorption are presented in Figure 2. The corresponding profiles from the other mixed oxide catalysts are included in the supplementary material (Figures S1–S3). Comparison of $Mn_{0.25}Ce_{0.75}$ with $CeO_2$ shows the following: (i) a broad CO peak with a low-temperature shoulder appears on $Mn_{0.25}Ce_{0.75}$ at ~380 °C instead of the three CO peaks over $CeO_2$; and (ii) $CO_2$ peaks have shifted to lower temperatures on $Mn_{0.25}Ce_{0.75}$, where they appear at 280 °C and 400 °C instead of 350–400 °C and 600–700 °C for $CeO_2$.

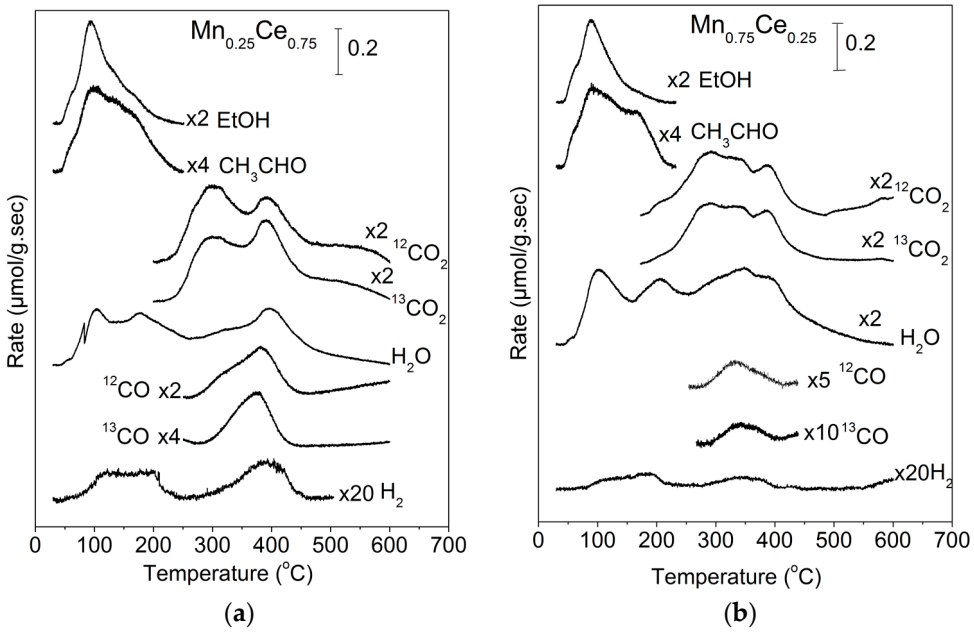


**Figure 2.** (**a**) TPD profiles following $^{12}CH_3{}^{13}CH_2OH$ adsorption on $Mn_{0.25}Ce_{0.75}$ catalyst, (**b**) TPD profiles following $^{12}CH_3{}^{13}CH_2OH$ adsorption on $Mn_{0.75}Ce_{0.25}$ catalyst.

Table 1 presents the product distribution during ethanol-TPD over $Mn_xCe_{1-x}$ catalysts calculated on a carbon mass balance basis according to Equation (4) (EtOH(%) is given as an example):

$$EtOH(\%) = 2y_{EtOH}/(2y_{EtOH} + 2y_{CH3CHO} + y_{CO2} + y_{CO}) \quad (4)$$

The amount of desorbed ethanol was 13% of the total carbon mass balance for $MnO_x$ and 28% for $CeO_2$. In a similar fashion, acetaldehyde was 12% for $MnO_x$ and 23% for $CeO_2$. The most important difference is in the case of $CO_2$, which is 71% for $MnO_x$ and only 28% for $CeO_2$, and also for CO, which is not present at all for $MnO_x$. The amount of hydrogen is quite low in all cases (most of the hydrogen atoms leave the surface in acetaldehyde and water), but again it is considerably less for $MnO_x$ than for $CeO_2$. The last column in Table 1 presents the percentage of $CO_2$ produced during exposure of the catalysts to oxygen at the end of the TPD run at 700 °C. It can be observed that a minor fraction (3–4%) of carbon from adsorbed ethanol remains on the surface at the end of TPD and is titrated as $CO_2$. Due to its small quantity, the residual carbon has not been taken into account in the carbon mass balance presented in Table 1.

**Table 1.** Product distribution during ethanol-TPD over $Mn_xCe_{1-x}$ catalysts.

| | EtOH (%) | $CH_3CHO$ (%) | $CO_2$ (%) | CO (%) | $H_2$ [a] (%) | $CO_2$ [b] (%) |
|---|---|---|---|---|---|---|
| $CeO_2$ | 28.1 | 22.7 | 28.1 | 21.9 | 6.8 | 3.1 |
| $Mn_{0.05}Ce_{0.95}$ | 17.7 | 19.0 | 47.2 | 15 | 1.6 | 2.6 |
| $Mn_{0.15}Ce_{0.85}$ | 15.5 | 15.8 | 53.1 | 14.1 | 1.4 | 0.6 |
| $Mn_{0.25}Ce_{0.75}$ | 14.6 | 15.9 | 59.6 | 7.9 | 0.8 | - |
| $Mn_{0.50}Ce_{0.50}$ | 13.0 | 15.3 | 60.3 | 7.9 | - | 0.3 |
| $Mn_{0.75}Ce_{0.25}$ | 13.0 | 21.5 | 62.5 | 2.8 | 0.6 | 0.3 |
| $MnO_x$ | 13.2 | 11.8 | 70.6 | - | 0.8 | 4.2 |

[a] Expressed as a percentage of the total amount of hydrogen contained in adsorbed ethanol. [b] It refers to the amount of $CO_2$ produced at the end of TPD experiment during exposure to oxygen.

### 2.2. Temperature-Programmed Oxidation (TPO) of Ethanol

Temperature programmed oxidation profiles of ethanol over pure $CeO_2$ and pure $MnO_x$ are presented in Figure 3. The presence of gaseous oxygen leads to the disappearance of CO and $H_2$, which get oxidized to $CO_2$ and $H_2O$, respectively, and the $CO_2$ peaks are shifted to lower temperatures. In the case of $CeO_2$, the $CO_2$ profile is rather broad with a peak below 300 °C, while the $CO_2$ peaks appeared above 350 °C in the absence of oxygen. In the case of $MnO_x$, the $CO_2$ peak is shifted from 340 °C to 223 °C. The profile of $O_2$ consumption closely follows the profile of oxidation products ($CO_2$, $H_2O$) in the case of $MnO_x$, but for $CeO_2$, a higher oxygen consumption is observed in the low-temperature range (100–200 °C) and this also applies to the water profile which does not have a peak at the same region as $CO_2$. This implies that oxidation of adsorbed ethanol takes place through an oxidative dehydrogenation step leading to water desorption and to a carbon-rich adsorbed intermediate which is oxidized to $CO_2$ at higher temperatures.

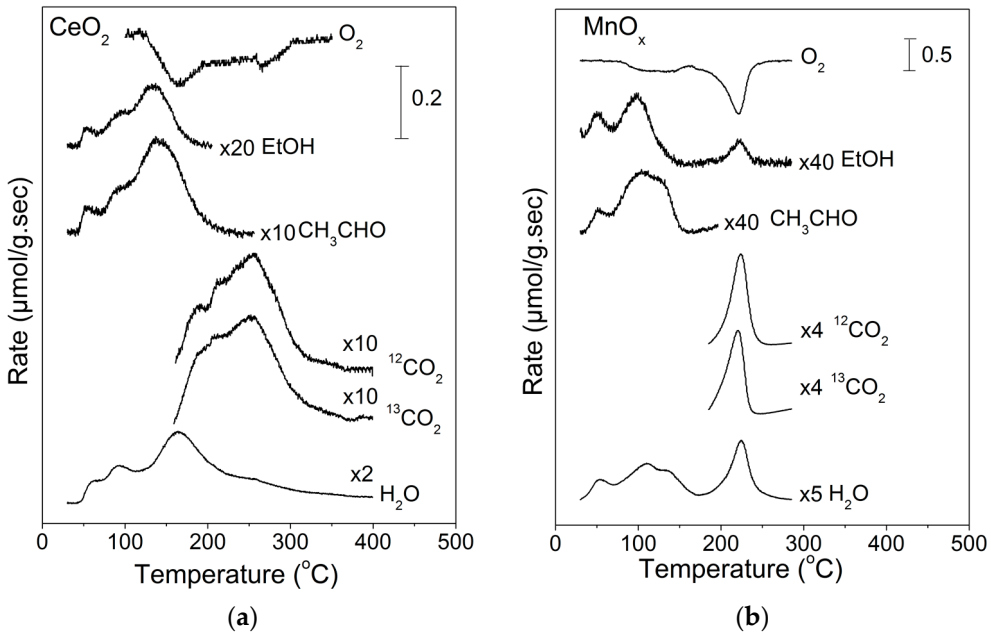


**Figure 3.** (**a**) TPO profiles following $^{12}CH_3{}^{13}CH_2OH$ adsorption on pure $CeO_2$, (**b**) TPO profiles following $^{12}CH_3{}^{13}CH_2OH$ adsorption on pure $MnO_x$.

The corresponding TPO profiles of ethanol from $Mn_{0.25}Ce_{0.75}$ and $Mn_{0.75}Ce_{0.25}$ catalysts following $^{12}CH_3{}^{13}CH_2OH$ adsorption are presented in Figure 4, while the TPO profiles from the other mixed oxide catalysts are included in the supplementary material (Figures S4–S6). The profiles from the Ce-rich and the Mn-rich catalysts bear many similarities, showing $^{13}CO_2$ and $CO_2$ peaks at around 240 °C.

The profiles of $H_2O$ are also similar and they consist of four peaks, from which the first three appearing below 200 °C coincide with acetaldehyde production and the fourth $H_2O$ peak coincides with $CO_2$ production. The profile of $O_2$ consumption coincides with the profiles of oxidation products ($H_2O$ and $CO_2$). Table 2 presents the product distribution of carbon-containing products during ethanol-TPO over $Mn_xCe_{1-x}$ catalysts. The amounts of desorbed ethanol were lower than those in TPD experiments (Table 1), indicating that gaseous oxygen has enhanced the oxidation ability of the catalysts and ceria was again the sample with the highest percentage of desorbed ethanol. Regarding acetaldehyde, its relative amount was slightly increased in most catalysts with the exception of ceria, where it remained stable. The amount of $CO_2$ increased considerably, especially in the case of ceria-rich catalysts. The $^{13}CO_2$ peak appears invariably at a lower temperature than the $^{12}CO_2$ peak by ~3 °C, indicating that the α-carbon of ethanol which is in a higher initial oxidation state gets more easily oxidized than the β-carbon.

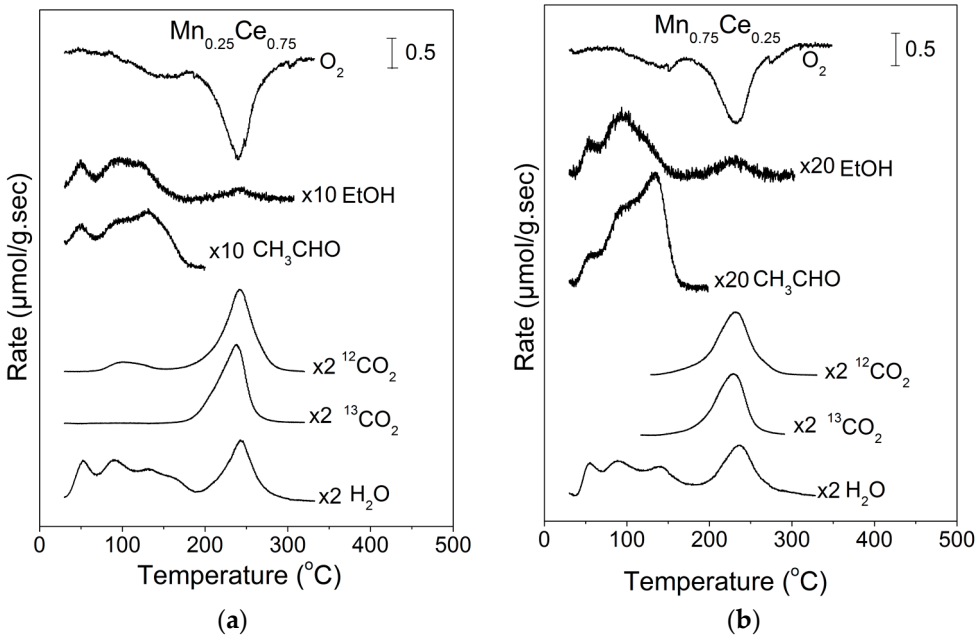


**Figure 4.** (**a**) TPO profiles following $^{12}CH_3{}^{13}CH_2OH$ adsorption on $Mn_{0.25}Ce_{0.75}$ catalyst, (**b**) TPO profiles following $^{12}CH_3{}^{13}CH_2OH$ adsorption on $Mn_{0.75}Ce_{0.25}$ catalyst.

**Table 2.** Product distribution during ethanol-TPO over $Mn_xCe_{1-x}$ catalysts.

| | EtOH (%) | $CH_3CHO$ (%) | $CO_2$ (%) |
|---|---|---|---|
| $CeO_2$ | 12.5 | 22.7 | 61.6 |
| $Mn_{0.05}Ce_{0.95}$ | 11.1 | 28.6 | 75.8 |
| $Mn_{0.15}Ce_{0.85}$ | 4.8 | 18.0 | 79.2 |
| $Mn_{0.25}Ce_{0.75}$ | 9.5 | 21.9 | 72.9 |
| $Mn_{0.50}Ce_{0.50}$ | 10.9 | 26.1 | 70.1 |
| $Mn_{0.75}Ce_{0.25}$ | 6.6 | 15.3 | 74.4 |
| $MnO_x$ | 6.3 | 15.9 | 80.8 |

One important indicator of the performance of the examined catalysts in the complete oxidation of ethanol is the profile of $CO_2$ during TPO, which is produced from oxidation of organic surface species originating from adsorbed ethanol. These $CO_2$ profiles are compiled in Figure 5 for all catalysts for ease of comparison. A vertical dotted line passing through the $CO_2$ peak of $MnO_x$ helps in observing the trends along the composition of the catalysts. The $CO_2$ peak over $MnO_x$ is at 223 °C. There is a gradual shift of the $CO_2$ peak to higher temperatures with an increase of cerium content. For example, the peak is at 230 °C for $Mn_{0.75}Ce_{0.25}$ and 251 °C for $Mn_{0.05}Ce_{0.95}$. In addition, there is a minor growth

of a low-temp $CO_2$ peak at 100–120 °C. The $CO_2$ profile over pure $CeO_2$ is quite different than all other Mn-containing samples. It is rather broad, with $CO_2$ already appearing at 50 °C and extending up to 350 °C. Nevertheless, the major $CO_2$ peak is at 256 °C. Therefore, the surface species originating from preadsorbed ethanol get oxidized to $CO_2$ with increasing difficulty with an increase of cerium content in the catalysts and $MnO_x$ is the sample with the highest intrinsic activity among all examined catalysts.

The other indicator of the catalytic performance is the concentration (or number density) of active sites on the surface. Since the studied reaction in this work is ethanol oxidation, ethanol can be taken to be the most reliable probe molecule to titrate the active sites. Thus the amount of adsorbed ethanol per unit surface area is assumed to reflect the active site concentration. An alternative option is the specific amount of $CO_2$ produced from the oxidation of surface ethanol-derived species during TPO, since this reflects the pool of surface intermediates that get fully oxidized. Figure 6 depicts the specific amount (in $\mu mol/m^2$) of adsorbed ethanol and $CO_2$ produced during TPO as a function of the composition of $Mn_xCe_{1-x}$ catalysts. Both ethanol and $CO_2$ have the same dependence on catalyst composition. It is evident that the concentration of active sites decreases considerably by ~50% upon the addition of Mn ions to ceria and then gradually increases with increase of Mn content. The pure oxides appear to possess a higher concentration of active sites than all the mixed oxides. Therefore, the addition of Mn ions to ceria or cerium ions to $MnO_x$ invariably leads to a decrease of the active site concentration.

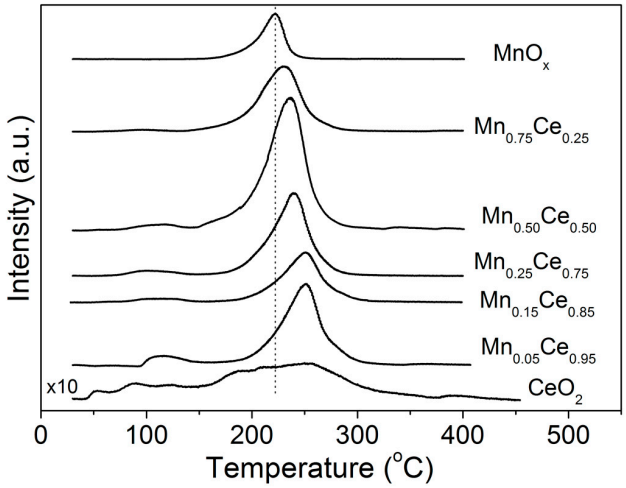


**Figure 5.** $CO_2$ profiles during TPO of ethanol over $Mn_xCe_{1-x}$ catalysts.

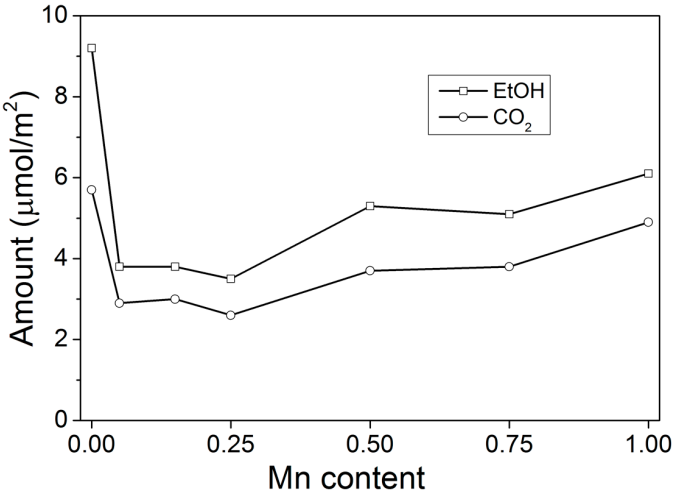


**Figure 6.** Specific amount of adsorbed ethanol and $CO_2$ produced during TPO as a function of the composition of $Mn_xCe_{1-x}$ catalysts.

## 3. Discussion

We have provided convincing experimental evidence that the density of active sites for ethanol oxidation is lower on mixed $Mn_xCe_{1-x}$ oxide catalysts compared to the corresponding pure oxides. In addition, the intrinsic activity of mixed oxides is lower than the one of pure $MnO_x$ and probably higher than pure $CeO_2$. The actual performance of mixed oxide catalysts under steady state conditions, however, is superior to the pure oxides [8] and the reaction rates per mass of catalyst are two to 10 times higher on mixed oxides. This is a direct consequence of the much larger specific surface area (SSA) of the mixed oxides (38–59 $m^2/g$ depending on Mn/Ce ratio, Table 3) compared to ~5 $m^2/g$ for pure $CeO_2$ and ~10 $m^2/g$ for pure $MnO_x$ [8]. The effect of SSA more than compensates for the unfavorable effects of the combination of the two oxides. Processing results presented in Ref. [8] in the light of the data of the present work leads to the calculation of the TOF of ethanol oxidation and the results are presented in Table 3. The TOF refers to the rate of ethanol consumption at 180 °C. It can be observed that pure $MnO_x$ is around four times more active than pure $CeO_2$. The TOF of all mixed oxides lies in between TOFs of the pure oxides. Focusing on the Ce-rich composition ($x$ up to 0.25) where manganese ions are incorporated into the ceria lattice forming a solid solution [8,27,28], it is evident that the addition of Mn ions leads to doubling of the TOF, but also to halving of the concentration of the active sites. At the same time, the SSA of Ce-rich mixed oxides is almost one order of magnitude higher than the one of pure $CeO_2$, indicating that the presence of manganese ions is beneficial for the containment of crystal growth during catalyst synthesis and preservation of the nanostructure [8,28,29]. "Dilution" of manganese oxide with ceria, on the other hand, leads to a decrease of intrinsic activity by 50% as well as to a decrease of the concentration of active sites, but again to an increase of SSA.

**Table 3.** Turnover Frequency (TOF) of ethanol oxidation at 180 °C over $Mn_xCe_{1-x}$ catalysts.

| Catalyst | SSA ($m^2\ g^{-1}$) | $C_{sites}$ ($\mu mol\ m^{-2}$) | R ($\mu mol\ s^{-1}\ g^{-1}$) | TOF ($\times 10^{-3}\ s^{-1}$) |
|---|---|---|---|---|
| $CeO_2$ | 4.8 | 9.2 | 0.07 | 1.52 |
| $Mn_{0.05}Ce_{0.95}$ | 59.4 | 3.8 | 0.35 | 1.57 |
| $Mn_{0.15}Ce_{0.85}$ | 50.0 | 3.8 | 0.56 | 2.95 |
| $Mn_{0.25}Ce_{0.75}$ | 47.3 | 3.5 | 0.50 | 3.03 |
| $Mn_{0.50}Ce_{0.50}$ | 48.8 | 5.3 | 0.73 | 2.81 |
| $Mn_{0.75}Ce_{0.25}$ | 38.2 | 5.1 | 0.75 | 3.86 |
| $MnO_x$ | 10.3 | 6.1 | 0.37 | 5.87 |

It is not an easy task to provide an explanation for the observed behavior of mixed $Mn_xCe_{1-x}$ oxides compared to pure $CeO_2$ or $MnO_x$. Trovarelli and Llorca have stressed the importance of size, shape, and degree of exposure of specific facets of ceria-based particles on their catalytic performance [30]. The distribution of specific nanofacets of ceria depends on its size and shape and leads to different reactivity in CO adsorption, for example [31]. Li et al. [14] have found that $MnO_x$-$CeO_2$ nanocubes exposing the {100} plane are twice as active in ethanol oxidation as $MnO_x$-$CeO_2$ nanorods primarily exposing the {111} plane. Therefore, it could be postulated that the observed behavior of mixed $Mn_xCe_{1-x}$ oxides in the present work is due to the different exposure of facets induced by the addition of manganese ions into ceria and the accompanying effect of smaller crystallite size of the mixed oxide samples. A similar trend concerning the effect of composition of $Mn_xCe_{1-x}$ catalysts on SSA, reaction rate, and specific activity has been observed by Chen et al. in the case of phenol wet oxidation [28]. In a broader context, it is a pity that data on differential reaction rates, specific reaction rates, and intrinsic activity (TOF) are scarcely reported in the relevant literature of ceria-based materials applied in VOC oxidation. Typically, the reported catalytic experiments consist of conversion curves as a function of reaction temperature and the indicators of catalytic activity are the $T_{10}$, $T_{50}$, and $T_{90}$ temperatures.

## 4. Materials and Methods

$MnO_x$-$CeO_2$ catalysts were prepared by the urea combustion method. Details of catalyst preparation can be found elsewhere [8]. For ease of reference, the catalysts are denoted as $Mn_xCe_{1-x}$, where $x$ is the Mn/(Mn + Ce) atomic ratio. Pure $MnO_x$ and $CeO_2$ samples were also prepared with the same method.

TPD and TPO experiments were performed in a fixed-bed reactor system interfaced to an on-line mass spectrometer (Omnistar, Pfeiffer Vacuum GmbH, Asslar, Germany). Isotopically-labelled ethanol, namely $^{12}CH_3{}^{13}CH_2OH$ (obtained from Sigma-Aldrich Chemie GmbH, Taufkirchen, Germany), was used in the present work.

The number of catalysts employed in the experiments was varied in order to keep the sample surface area loaded in the reactor fixed at 2.5 $m^2$. The corresponding amounts varied between 42 mg for $Mn_{0.05}Ce_{0.95}$ (sample with highest specific surface area) and 520 mg for $CeO_2$ (sample with lowest specific surface area). Table 3 presents the specific surface areas for all examined catalysts. Prior to each TPD or TPO run, the catalyst sample was treated under a flow of 20% $O_2$/He at 550 °C for half an hour and was subsequently cooled to room temperature under He flow. This procedure was found to give reproducible results. Ethanol was adsorbed on the catalyst surface at room temperature from a flow of He containing ~1600 ppm of ethanol. The feed also contained 2% Ar as an inert tracer. Following completion of ethanol adsorption, as indicated by the stable signal of ethanol in the mass spectrometer, the catalyst was purged with helium to remove any weakly adsorbed ethanol from the surface, as well as to purge ethanol vapors from the reactor and lines. Then, temperature programming was commenced with a heating rate of 10 °C $min^{-1}$ up to 600 °C. Helium was used as the carrier gas for TPD and a 1%$O_2$/He mixture for TPO, with a flow rate of 50 $cm^3$ $min^{-1}$ in both cases. At the end of the TPD runs and while the catalyst was maintained at 600 °C, the flow was switched to a 1% $O_2$/He mixture in order to titrate possible carbonaceous residues on the catalyst originating from ethanol. Preliminary TPD and TPO experiments were conducted on all catalysts in order to identify the compounds appearing in the gas phase during the run. This was accomplished by continuous scanning of mass numbers ($m/z$) from 1 to 100 during heating. Ethanol and acetaldehyde were the only organic molecules detected during TPD and TPO. Corrections for cracking in the mass spectrometer were made for each product, and for some species, multiple corrections were necessary. Each species signal, except for those containing $^{13}C$, was calibrated with the use of gaseous mixtures of a known composition. Products containing $^{13}C$ were calibrated by using the equivalent $^{12}C$ compounds.

## 5. Conclusions

The interaction of ethanol with $Mn_xCe_{1-x}$ catalysts has been investigated with TPD and TPO techniques. It has been found that the addition of Mn ions to ceria leads to:

- A decrease of the concentration of active sites, on the hypothesis that the amount of adsorbed ethanol and produced $CO_2$ during TPO are proper probes for counting these sites
- Doubling of TOF for ethanol oxidation.

On the other hand, the addition of cerium ions to $MnO_x$ leads to:

- A decrease of the concentration of active sites
- A decrease of TOF for ethanol oxidation by ~50%.

The significantly higher SSA of the mixed oxides more than compensates for the observed variations in intrinsic activity and density of active sites.

**Supplementary Materials:** The following are available online at www.mdpi.com/2073-4344/7/11/339/s1, Figure S1: TPD profiles following $^{12}CH_3{}^{13}CH_2OH$ adsorption on $Mn_{0.05}Ce_{0.95}$ catalyst, Figure S2: TPD profiles following $^{12}CH_3{}^{13}CH_2OH$ adsorption on $Mn_{0.15}Ce_{0.85}$ catalyst, Figure S3: TPD profiles following $^{12}CH_3{}^{13}CH_2OH$ adsorption on $Mn_{0.50}Ce_{0.50}$ catalyst, Figure S4: TPO profiles following $^{12}CH_3{}^{13}CH_2OH$ adsorption on $Mn_{0.05}Ce_{0.95}$

catalyst, Figure S5: TPO profiles following $^{12}CH_3{}^{13}CH_2OH$ adsorption on $Mn_{0.15}Ce_{0.85}$ catalyst, Figure S6: TPO profiles following $^{12}CH_3{}^{13}CH_2OH$ adsorption on $Mn_{0.50}Ce_{0.50}$ catalyst.

**Author Contributions:** D.D. performed the experiments and analyzed the data; T.I. wrote the paper.

**Conflicts of Interest:** The authors declare no conflict of interest.

## References


1. Spivey, J.J. Complete catalytic oxidation of volatile organics. *Ind. Eng. Chem. Res.* **1987**, *27*, 2165–2180. [CrossRef]
2. Cordi, E.M.; Falconer, J.L. Oxidation of volatile organic compounds on $Al_2O_3$, $Pd/Al_2O_3$, and $PdO/Al_2O_3$ catalysts. *J. Catal.* **1996**, *162*, 104–117. [CrossRef]
3. Liotta, L.F. Catalytic oxidation of volatile organic compounds on supported noble metals. *Appl. Catal. B Environ.* **2010**, *100*, 403–412. [CrossRef]
4. Avgouropoulos, G.; Oikonomopoulos, E.; Kanistras, D.; Ioannides, T. Complete oxidation of ethanol over alkali-promoted $Pt/Al_2O_3$ catalysts. *Appl. Catal. B Environ.* **2006**, *65*, 62–69. [CrossRef]
5. Larsson, P.O.; Andersson, A. Complete oxidation of CO, ethanol, and ethyl acetate over copper oxide supported on Titania and ceria modified Titania. *J. Catal.* **1998**, *179*, 72–89. [CrossRef]
6. Kamal, M.S.; Shaikh, A.; Razzak, S.A.; Hossain, M.M. Catalytic oxidation of volatile organic compounds (VOCs)—A review. *Atmos. Environ.* **2016**, *140*, 117–134. [CrossRef]
7. Xu, H.; Yan, N.; Qu, Z.; Liu, W.; Mei, J.; Huang, W.; Zhao, S. Gaseous heterogeneous catalytic reactions over Mn-Based Oxides for environmental applications: A critical review. *Environ. Sci. Technol.* **2017**, *51*, 8879–8892. [CrossRef] [PubMed]
8. Delimaris, D.; Ioannides, T. VOC oxidation over $MnO_x$-$CeO_2$ catalysts prepared by a combustion method. *Appl. Catal. B Environ.* **2008**, *84*, 303–312. [CrossRef]
9. Lin, P.; Luo, M.-F.; Xin, Q.; Sun, G.-Q. The mechanism studies of ethanol oxidation on PdO catalysts by TPSR techniques. *Catal. Lett.* **2004**, *93*, 139–144. [CrossRef]
10. Idriss, H.; Diagne, C.; Hindermann, J.P.; Kiennemann, A.; Barteau, M.A. Reactions of acetaldehyde on $CeO_2$ and $CeO_2$-Supported catalysts. *J. Catal.* **1995**, *155*, 219–237. [CrossRef]
11. Yee, A.; Morrison, S.J.; Idriss, H. A study of the reactions of ethanol on $CeO_2$ and $Pd/CeO_2$ by steady state reactions, temperature programmed desorption, and in situ FT-IR. *J. Catal.* **1999**, *186*, 279–295. [CrossRef]
12. Yee, A.; Morrison, S.J.; Idriss, H. A study of ethanol reactions over $Pt/CeO_2$ by temperature-programmed desorption and in situ FT-IR spectroscopy: Evidence of benzene formation. *J. Catal.* **2000**, *191*, 30–45. [CrossRef]
13. De Lima, S.M.; da Silva, A.M.; da Costa, L.O.O.; Graham, U.M.; Jacobs, G.; Davis, B.H.; Mattos, L.V.; Noronha, F.B. Study of catalyst deactivation and reaction mechanism of steam reforming, partial oxidation, and oxidative steam reforming of ethanol over $Co/CeO_2$ catalyst. *J. Catal.* **2009**, *268*, 268–281. [CrossRef]
14. Li, H.; Qi, G.; Tana; Zhang, X.; Li, W.; Shen, W. Morphological impact of manganese–cerium oxides on ethanol oxidation. *Catal. Sci. Technol.* **2011**, *1*, 1677–1682. [CrossRef]
15. Li, H.; Qi, G.; Tana; Zhang, X.; Huang, X.; Li, W.; Shen, W. Low-temperature oxidation of ethanol over a $Mn_{0.6}Ce_{0.4}O_2$ mixed oxide. *Appl. Catal. B Environ.* **2011**, *103*, 54–61. [CrossRef]
16. Liu, G.; Yue, R.; Jia, Y.; Ni, Y.; Yang, J.; Liu, H.; Wang, Z.; Wu, X.; Chen, Y. Catalytic oxidation of benzene over Ce–Mn oxides synthesized by flame spray pyrolysis. *Particuology* **2013**, *11*, 454–459. [CrossRef]
17. Liao, Y.; Fu, M.; Chen, L.; Wu, J.; Huang, B.; Ye, D. Catalytic oxidation of toluene over nanorod-structured Mn–Ce mixed oxides. *Catal. Today* **2013**, *216*, 220–228. [CrossRef]
18. Tang, W.; Wu, X.; Liu, G.; Li, S.; Li, D.; Li, W.; Chen, Y. Preparation of hierarchical layer-stacking Mn-Ce composite oxide for catalytic total oxidation of VOCs. *J. Rare Earths* **2015**, *33*, 62–69. [CrossRef]
19. Tang, W.; Wu, X.; Li, S.; Li, W.; Chen, Y. Porous Mn-Co mixed oxide nanorod as a novel catalyst with enhanced catalytic activity for removal of VOCs. *Catal. Commun.* **2014**, *56*, 134–138. [CrossRef]
20. Picasso, G.; Cruz, R.; del Rosario Sun Kou, M. Preparation by co-precipitation of Ce-Mn based catalysts for combustion of n-hexane. *Mater. Res. Bull.* **2015**, *70*, 621–632. [CrossRef]
21. Chojnacka, A.; Molenda, M.; Chmielarz, L.; Piwowarska, Z.; Gajewska, M.; Dudek, B.; Dziembaj, R. Ceria based novel nanocomposites catalysts $Mn_xCe_{1-x}$ $O_2/\alpha$-$Al_2O_3$ for low-temperature combustion of methanol. *Catal. Today* **2015**, *257*, 104–110. [CrossRef]

22. Zhao, H.; Zhou, X.; Wang, M.; Xie, Z.; Chen, H.; Shi, J. Highly active $MnO_x$–$CeO_2$ catalyst for diesel soot combustion. *RSC Adv.* **2017**, *7*, 3233–3239. [CrossRef]
23. Colman-Lerner, E.; Peluso, M.A.; Sambeth, J.; Thomas, H. Cerium, manganese and cerium/manganese ceramic monolithic catalysts. Study of VOCs and PM removal. *J. Rare Earths* **2016**, *34*, 675–682. [CrossRef]
24. Pintos, D.G.; Juan, A.; Irigoyen, B. Mn-Doped $CeO_2$: DFT+U Study of a Catalyst for Oxidation Reactions. *J. Phys. Chem. C* **2013**, *117*, 18063–18073. [CrossRef]
25. Vannice, M.A. *Kinetics of Catalytic Reactions*, 1st ed.; Springer: New York, NY, USA, 2005; pp. 6–8. ISBN 978-1-4419-3758-2.
26. Sheng, P.-Y.; Bowmaker, G.A.; Idriss, H. The Reactions of Ethanol over $Au/CeO_2$. *Appl. Catal. A Gen.* **2004**, *261*, 171–181. [CrossRef]
27. Machida, M.; Uto, M.; Kurogi, D.; Kijima, T. $MnO_x$-$CeO_2$ Binary Oxides for Catalytic $NO_x$ Sorption at Low Temperatures. Sorptive Removal of $NO_x$. *Chem. Mater.* **2000**, *12*, 3158–3164. [CrossRef]
28. Chen, H.; Sayari, A.; Adnot, A.; Larachi, F. Composition–activity effects of Mn-Ce-O composites on phenol catalytic wet oxidation. *Appl. Catal. B Environ.* **2001**, *32*, 195–204. [CrossRef]
29. Picasso, G.; Gutiérrez, M.; Pina, M.P.; Herguido, J. Preparation and characterization of Ce-Zr and Ce-Mn based oxides for n-hexane combustion: Application to catalytic membrane reactors. *Chem. Eng. J.* **2007**, *126*, 119–130. [CrossRef]
30. Trovarelli, A.; Llorca, J. Ceria Catalysts at Nanoscale: How Do Crystal Shapes Shape Catalysis? *ACS Catal.* **2017**, *7*, 4716–4735. [CrossRef]
31. Yang, C.; Yu, X.; Heißler, S.; Nefedov, A.; Colussi, S.; Llorca, J.; Trovarelli, A.; Wang, Y.; Wöll, C. Surface Faceting and Reconstruction of Ceria Nanoparticles. *Angew. Chem. Int. Ed.* **2017**, *56*, 375–379. [CrossRef] [PubMed]